Quantum heat valve and diode of strongly coupled defects in amorphous material

Yu-qiang Liu, Yi-jia Yang, Ting-ting Ma, Zheng Liu, and Chang-shui Yu*
School of Physics, Dalian University of Technology, Dalian 116024, People's Republic of China

(Received 27 July 2023; accepted 20 December 2023; published 26 January 2024)

The mechanical strain can control the frequency of two-level atoms in amorphous material. In this work, we would like to employ two coupled two-level atoms to manipulate the magnitude and direction of heat transport by controlling mechanical strain to realize the function of a thermal switch and valve. It is found that a high-performance heat diode can be realized in the wide piezo voltage range at different temperatures. We also discuss the dependence of the rectification factor on temperatures and couplings of heat reservoirs. We find that the higher temperature differences correspond to the larger rectification effect. The asymmetry system-reservoir coupling strength can enhance the magnitude of heat transfer, and the impact of asymmetric and symmetric coupling strength on the performance of the heat diode is complementary. It may provide an efficient way to modulate and control heat transport's magnitude and flow preference. This work may give insight into designing and tuning quantum heat machines.

DOI: 10.1103/PhysRevE.109.014137

I. INTRODUCTION

The theoretical and experimental advances of quantum heat transport, including heat conductance and control by external fields, lead to the rapid development of quantum thermodynamics [1]. Moreover, recent advances in the superconducting quantum circuit [2–4] based on flexibility and scalability have provided new insight into quantum heat transport [1,5] and quantum thermodynamics [6]. Besides, manipulating electronic heat current in solid-state thermal circuits also provides a reference for the control heat current in quantum systems [7]. The manipulation and control of heat current at the quantum level as a basic research field of quantum thermodynamics have been significant progress. So far, various forms of quantum thermal machines have been proposed and designed, such as refrigerators and heat engines [8–14], rectifier [15–28], transistor [29–35], thermometer [36,37], valve [38,39], and attracted extensive attention from plenty of researchers. As a vital part of thermal machines, thermal rectification devices mainly refer to diodes and transistors. As a two-terminal device, a quantum thermal diode can induce heat flows inclined in one direction. As a three-terminal device, quantum thermal transistors can realize that a weak heat current can amplify the heat currents of the two other terminals. Quantum thermal diodes and transistors are analogous to their electronic counterpart and have been designed in plenty of systems such as atoms [16,17,29,30,33,40,41], quantum circuits [22,28,32], spin chains [18–21], and quantum dots [15,24,34]. These proposals mainly focus on the modulation of the temperature of the reservoirs. A natural question arises as to whether or not other proposals exist to realize the manipulation of heat transport.

In recent years, some researchers have tried to explore other modulation forms of heat transport, such as period driving and external magnetic flux. Gupt *et al.* employ periodic control to realize a quantum thermal transistor [31]. Portugal *et al.* research heat transport using a two-level system via a periodically modulated temperature [42]. Karimi *et al.* [43] employ two superconducting qubits to design a flux-modulation heat switch. Ronzani *et al.* realize a heat valve with a transmon qubit by modulating the applied magnetic flux [38]. Xu *et al.* discuss heat transfer with an external magnetic flux tunable transmon qubit [23]. Senior *et al.* design a magnetic flux-controled heat diode [44]. In this context, researching different modulation ways of heat current has gradually become a promising topic. Recently, Lisenfeld *et al.* first directly and experimentally observed two strongly interacting and coherent two-level systems embedding in the tunnel barrier of a Josephson junction (JJ) by modulating the mechanical strain [45]. Also, a two-level system or small group of atoms in an amorphous material is one of the most promising models [46,47]. In addition, the two-level defect can also be coupled with the optomechanical system to achieve phonon blockade and preparation of nonclassical states. [48]. Given that the changes of two-level atom frequencies depend on the applied piezo voltage, it is advantageous to employ the piezo voltage to control the heat transport for realizing some function. Inspired by this, we will use this coupled defect system to design a mechanical strain-controlled heat valve and diode in amorphous solids.

This work considers the coupling defects to design a perfect heat diode and controllable heat valve. We first show that a well-performance heat valve and diode can be realized by modulating the piezo voltage, and the maximal rectification can be obtained when considering the resonant case. We find that a large rectification effect can be discovered at resonant frequencies with a large temperature bias. Next, we investigate how the asymmetric system-reservoir coupling strength

*ycs@dlut.edu.cn

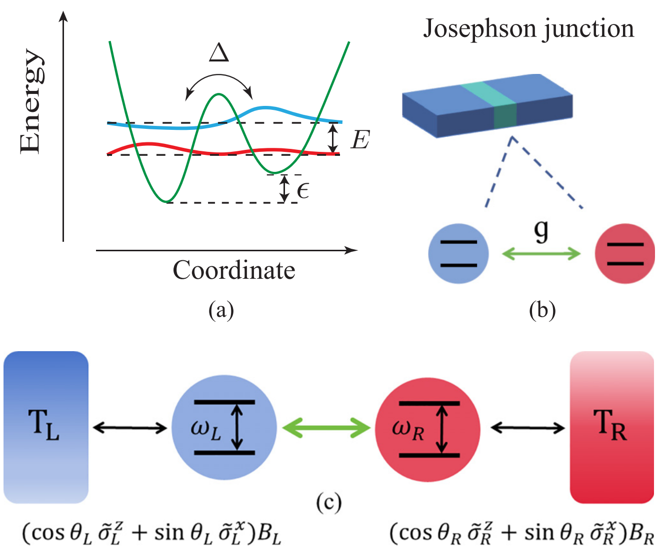

FIG. 1. (a) The double-well potential system in the two-level atom limit. Δ, ϵ denote the tunneling energy and asymmetry energy, and E is the level splitting with $E=\sqrt{\Delta^2+\epsilon^2}$. (b) The model consists of two coherent coupling two-level atoms embedding in the tunnel barrier of a Josephson junction (JJ). (c) Schematic diagram of quantum heat diode and valve. Intuitively, the mechanism of asymmetry of heat transport can be roughly understood in two contributions: the off-resonantly interacting atoms and the different system-reservoir couplings.

further influences the performance of the heat valve and diode. We find that the stronger asymmetric coupling strength can realize the larger heat transport, and the performance of heat diodes employing asymmetric and symmetric couplings can be complementary. Besides, we also discuss the dependence of the performance of a heat diode on temperature and find that the higher temperature difference allows for greater heat current rectification.

The structure of this paper is organized as follows. In Sec. II, we introduce the Hamiltonian of two coupled two-level atoms and their dissipation and derive the global master equation. In Sec. III, we discuss a modulated heat valve and the realization parameters range of perfect rectification. The conclusion is given in Sec. IV.

II. PHYSICAL MODEL AND DYNAMICS

Josephson junctions consist of aluminum, and its oxide has become a common functional element in the design of superconducting circuits [49]. In general, the disordered thin film AlOx of the junction exists in atomic tunneling systems, and it is described by a double-well system in the two-state limit, as shown in Fig. 1(a). We follow the model consisting of two coherent coupling two-level atoms embedding in the tunnel barrier of a Josephson junction (JJ) in Fig. 1(b), and the details can refer to Refs. [45,50]. The Hamiltonian of the coupling two atoms can read as [45,50] ($\hbar=k_B=1$),

$$H_S=\frac{1}{2}\sum_{\mu=L,R}\left[\varepsilon_\mu\sigma_\mu^z+\Delta_\mu\sigma_\mu^x\right]+\frac{1}{2}g\sigma_L^z\sigma_R^z, \tag{1}$$

where σ_μ^z, σ_μ^x are Pauli spin operators, Δ_μ denote the tunneling energy, ε_μ are the asymmetry energy, and g is the coupling strength of two atoms. Experimentally, one can slightly bend the sample chip by employing a piezo actuator to manipulate and control the asymmetry energy *in situ* $\varepsilon_\mu=\varepsilon_\mu(V_p)=c_\mu(V_p-V_{0\mu})$ [46,51]. A unitary transformation can lead to this equation

$$\sigma_\mu^z\rightarrow\cos\theta_\mu\tilde{\sigma}_\mu^z+\sin\theta_\mu\tilde{\sigma}_\mu^x, \tag{2}$$

and the corresponding system Hamiltonian (1) can also be transformed as

$$\tilde{H}_S=\frac{\omega_L}{2}\tilde{\sigma}_L^z+\frac{\omega_R}{2}\tilde{\sigma}_R^z+\frac{g_\parallel}{2}\tilde{\sigma}_L^z\tilde{\sigma}_R^z+\frac{g_\perp}{2}\tilde{\sigma}_L^x\tilde{\sigma}_R^x, \tag{3}$$

where $\omega_\mu=\sqrt{\varepsilon_\mu^2(V_p)+\Delta_\mu^2}$, $g_\parallel=g\cos\theta_L\cos\theta_R$, and $g_\perp=g\sin\theta_L\sin\theta_R$ where $\cos\theta_\mu=\varepsilon_\mu/\omega_\mu$ denotes transversal and longitudinal coupling, respectively, and they are easily identifiable in experiment [45], as well as two minor energy shifts terms can be neglected [45,50]. One can diagonalize the system Hamiltonian (3), and the eigenvalues can read as

$$\begin{aligned}\epsilon_{1,2}&=\mp\frac{1}{2}\sqrt{(\omega_L+\omega_R)^2+g_\perp^2}+\frac{g_\parallel}{2},\\ \epsilon_{3,4}&=\pm\frac{1}{2}\sqrt{(\omega_L-\omega_R)^2+g_\perp^2}-\frac{g_\parallel}{2}.\end{aligned} \tag{4}$$

We can express it as a vector form $|\epsilon\rangle=[\epsilon_1,\epsilon_2,\epsilon_3,\epsilon_4]^{\mathrm{T}}$, and the corresponding eigenstates are

$$\begin{aligned}|\epsilon_1\rangle&=\cos(\alpha/2)|g,g\rangle-\sin(\alpha/2)|e,e\rangle,\\ |\epsilon_2\rangle&=\cos(\alpha/2)|e,e\rangle+\sin(\alpha/2)|g,g\rangle,\\ |\epsilon_3\rangle&=\cos(\beta/2)|e,g\rangle+\sin(\beta/2)|g,e\rangle,\\ |\epsilon_4\rangle&=\cos(\beta/2)|g,e\rangle-\sin(\beta/2)|e,g\rangle,\end{aligned} \tag{5}$$

with $\tan\alpha=\frac{g_\perp}{\omega_L+\omega_R}$, $\tan\beta=\frac{g_\perp}{\omega_L-\omega_R}$.

The system inevitably dissipates the energy to the external environment. We let the two atoms couple to an independent reservoir. In general, the environment can be modeled by a collection of independent harmonic oscillators, and the free Hamiltonian can read as [52]

$$\tilde{H}_R=\sum_\mu\omega_{\mu k}c_{\mu k}^\dagger c_{\mu k}, \tag{6}$$

where $\omega_{\mu k}$ denotes the frequency of reservoir μ at mode kth, and $c_{\mu k}$, $c_{\mu k}^\dagger$ are bosonic annihilation and creation operators of the reservoir modes. The reservoir can be modeled by the normal-metal resistor [44] or a general noiseless resistor with a fluctuating voltage source [53,54]. We can follow a Caldeira-Leggett-type system-bath Hamiltonian [55–58]

$$\tilde{H}_{S-R}=B_{\mathrm{L}}\left(\sigma_L^z\otimes 1\right)+B_{\mathrm{R}}\left(1\otimes\sigma_R^z\right), \tag{7}$$

where $B_\mu=\sum_k\kappa_{\mu k}(c_{\mu k}+c_{\mu k}^\dagger)$ and $\kappa_{\mu k}$ represents the coupling strength of the atom reservoir. The coupling of Eq. (7) is described by a spectral density [59]

$$J(\omega)=\sum_k\kappa_k^2\delta(\omega-\omega_k). \tag{8}$$

Hence, one can obtain the full Hamiltonian of system, environment, and their interaction,

$$H = \tilde{H}_S + \tilde{H}_R + \tilde{H}_{S-R}. \tag{9}$$

With transformation (2), the system-reservoir interaction Hamiltonian (7) can be rewritten as

$$H_{S-R} = B_{\rm L}(S_L \otimes 1) + B_{\rm R}(1 \otimes S_R), \tag{10}$$

with transformed jump operators $S_\mu = \cos\theta_\mu \tilde{\sigma}_\mu^z + \sin\theta_\mu \tilde{\sigma}_\mu^x$. In H_S representation, the total Hamiltonian (9) can be rewritten as

$$H = \sum_{j=1}^{4} |\epsilon_j\rangle\langle\epsilon_j| + \tilde{H}_R + H'_{S-R}, \tag{11}$$

and

$$H'_{S-R} = \sum_{\mu,k,l} \kappa_{\mu k}\big[c_{\mu k}^\dagger S_{\mu l}(\omega_{\mu l}) + c_{\mu k} S_{\mu l}^\dagger(\omega_{\mu l})\big]. \tag{12}$$

Here the eigenoperators $S_{\mu l}$ satisfy the commutation relation, $[H_S, S_{\mu l}] = -\omega_{\mu l} S_{\mu l}$, and $\omega_{\mu l}$ are the corresponding eigenfrequencies with subscript $l = 0, 1, 2, 3, 4, 5, 6$ shown in Appendix A. Note that the values of $\omega_{\mu l}$ depends on the different transition channels $|\epsilon_j\rangle \leftrightarrow |\epsilon_m\rangle$.

To study the dynamics of the system, we follow the stand method to derive the master equation based on Born-Markov-secular approximation, and the Lindblad form in the Schrödinger picture can be written as [60]

$$\dot{\rho} = -i[H_S, \rho] + \mathcal{L}_L[\rho] + \mathcal{L}_R[\rho], \tag{13}$$

where the dissipator $\mathcal{L}_\mu[\rho]$ is given by

$$\begin{aligned}\mathcal{L}_\mu[\rho] = \sum_{l=0}^{6} & J_\mu(-\omega_{\mu l})\big[2S_{\mu l}(\omega_{\mu l})\rho S_{\mu l}^\dagger(\omega_{\mu l}) \\ & - \big\{S_{\mu l}^\dagger(\omega_{\mu l})S_{\mu l}(\omega_{\mu l}), \rho\big\}\big] \\ & + J_\mu(\omega_{\mu l})\big[2S_{\mu l}^\dagger(\omega_{\mu l})\rho S_{\mu l}(\omega_{\mu l}) \\ & - \big\{S_{\mu l}(\omega_{\mu l})S_{\mu l}^\dagger(\omega_{\mu l}), \rho\big\}\big],\end{aligned} \tag{14}$$

where the spectral densities can take $J_\mu(\pm\omega_{\mu l}) = \gamma_\mu(\omega_{\mu l}) n_\mu(\pm\omega_{\mu l})$ with $\gamma_\mu(\omega) = \sum_k |\kappa_{\mu k}|^2 \delta(\omega - \omega_{\mu k})$ [61], and $n_\mu(\omega) = \frac{1}{\exp(\frac{\omega}{T_\mu})-1}$ is a Bose-Einstein function. We assume the dissipation rates are independent of frequencies for simplification, i.e., $\gamma_\mu(\omega_{\mu l}) = \gamma_\mu$. In the system representation, the master equation (13) is divided into diagonal and off-diagonal entries of the density operator. At steady-state, the only diagonal elements of the density matrix, termed populations [28,62], can remain, and the differential equation for the diagonal entries ρ_{jj} read as

$$\dot{\rho}_{jj} = \sum_\mu \sum_m \Gamma_{jm}^\mu(\rho), \tag{15}$$

where

$$\Gamma_{jm}^\mu(\rho) = \gamma_\mu[(n_\mu(\omega_{jm}) + 1)\rho_{mm} - n_\mu(\omega_{jm})\rho_{jj}]|\langle\epsilon_j|S_\mu|\epsilon_m\rangle|^2$$

with $\omega_{jm} = \epsilon_m - \epsilon_j$ representing the increment rate of the population ρ_{jj}. The evolution of the density matrix (15) can rewrite as $\frac{d|\rho_{ss}\rangle}{dt} = M|\rho_{ss}\rangle$ with $|\rho_{ss}\rangle = [\rho_{11}, \rho_{22}, \rho_{33}, \rho_{44}]^T$ and the matrix $M = \sum_\mu M_\mu$ [18]. The matrix M_μ is expressed as

$$M_\mu = \begin{pmatrix} M_{11}^\mu & A_{\mu 2} & A_{L4} & A_{\mu 6} \\ B_{\mu 2} & M_{22}^\mu & B_{\mu 1} & B_{\mu 3} \\ B_{\mu 4} & A_{\mu 1} & M_{33}^\mu & B_{\mu 5} \\ B_{\mu 6} & A_{\mu 3} & A_{\mu 5} & M_{44}^\mu \end{pmatrix}, \tag{16}$$

where $M_{11}^\mu = -\sum_{l=2,4,6} B_{\mu l}$, $M_{22}^\mu = -\sum_{l=1}^{3} A_{\mu l}$, $M_{33}^\mu = -B_{\mu 1} - \sum_{l=4,5} A_{\mu l}$, and $M_{44}^\mu = -\sum_{l=3,5} B_{\mu 3} - A_{\mu 6}$ with $A_{\mu l} = 2J_\mu(-\omega_{\mu l})a_{\mu l}^2$, $B_{\mu l} = 2J_\mu(\omega_{\mu l})a_{\mu l}^2$. Let $\frac{d|\rho_{ss}\rangle}{dt} = 0$; one will obtain the steady-state ρ_{ss}. Here, we focus on the thermodynamical behavior in the long time limit; the definition of heat current can be considered as follows [60]:

$$\dot{\mathcal{Q}}_\mu = {\rm Tr}\{H_S \mathcal{L}[\rho_{ss}]\}, \tag{17}$$

where $\dot{\mathcal{Q}}_\mu > 0$ denotes heat current transfer from reservoir μ to the system. The expression of heat current Eq. (17) can also be expressed as

$$\dot{\mathcal{Q}}_\mu = -\sum_{jm} \Gamma_{jm}^\mu(\rho_{ss})\omega_{jm} = \langle\epsilon|M_\mu|\rho_{ss}\rangle, \tag{18}$$

where transition energy $\omega_{jm} = \epsilon_m - \epsilon_j$, and the transition rates $\Gamma_{jm}^\mu(\rho_{ss}) = A_{\mu l}\rho_{jj} - B_{\mu l}\rho_{mm}$, defined before. As for a quantum heat diode, its performance can be characterized by a rectification factor, and it is defined as [18]

$$R = \frac{|\dot{\mathcal{Q}}_f + \dot{\mathcal{Q}}_r|}{|\dot{\mathcal{Q}}_f - \dot{\mathcal{Q}}_r|}. \tag{19}$$

We refer to the forward (reverse) heat current as $\dot{\mathcal{Q}}_{f/r} = \dot{\mathcal{Q}}_R$ and $\dot{\mathcal{Q}}_f \geqslant 0$, if $T_R \geqslant T_L$, and vice versa. This factor reflects the imbalance between the two directions of heat current when exchanging temperatures of two terminals. The range of R can take $0 \leqslant R \leqslant 1$; there is no rectification if $R = 0$, a perfect diode when $R = 1$, and a well-performing diode when $0 < R < 1$.

III. RESULTS AND DISCUSSIONS

In the simulation, we consider a strong internal coupling regime $g \sim 850$ MHz and follow the experimental parameters of Refs. [45,50,51,63] unless we stress. The related system parameters are as follows: the tunneling energy $\Delta_L = 7.5$ GHz, $\Delta_R = 1.3$ GHz; the asymmetry energy $\varepsilon_L = c_L V_p - 3.3$ [GHz], $\varepsilon_R(V_p) = c_R(V_p + 13[\text{V}])$, $c_L = 5\,\text{MHzV}^{-1}$, $c_R = 0.3$ GHzV^{-1}, and the internal coupling strength $g = 850$ MHz. As shown in Fig. 2, we plot the frequencies ω_μ versus the piezo voltage V_p. It is found that ω_L is nearly kept constant, but ω_R increases first and then decreases as piezo voltage V_p increases. Under such a parameter condition, modulating V_p can significantly change the frequency ω_R. Thus, one can modulate the voltage to change the frequency and further modulate the heat currents. We plot the heat current as a function of piezo voltage shown in Figs. 3(a) and 3(b). From Figs. 3(a) and 3(b), we find that

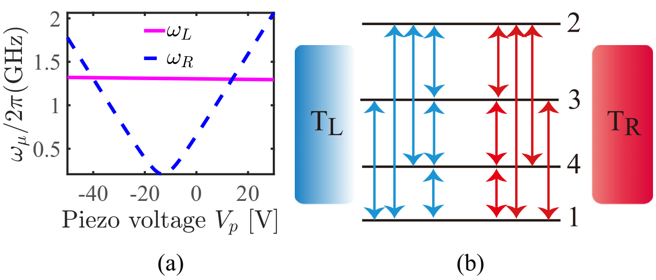

FIG. 2. (a) The Bohr frequencies ω_μ versus the piezo voltage V_P; (b) transition channels of open system. System parameters: the tunneling energy $\Delta_L = 7.5\,\text{GHz}$ and $\Delta_R = 1.3\,\text{GHz}$; the asymmetry energy $\varepsilon_L = c_L V_p - 3.3\,[\text{GHz}]$ and $\varepsilon_R(V_p) = c_R(V_p + 13[\text{V}])$; $c_L = 5\ \ \text{MHzV}^{-1}$ and $c_R = 0.3\,\text{GHzV}^{-1}$, the coupling strength $g = 850\,\text{MHz}$.

heat currents show nonmonotonic behavior, and the variation of temperature bias can enhance the magnitude of heat transfer, i.e., the higher temperature bias, the larger heat current. The maximal heat transport in Fig. 3(a) can be realized at $V_p = -40.3\ \ \text{V}$ and $V_p = 13.9\,\text{V}$ for resonant case $\omega_L = \omega_R$. It indicates the resonant condition not only realizing the large energy exchange with thermal reservoirs but also achieving the large rectification effects, which is similar to Ref. [25]. When we consider the reverse heat transport, heat currents closely resembled the forward case in low temperatures with $T_L = 0.5\,\text{K}, 1\,\text{K}$. Still, the higher temperatures at $T_L = 5\ \ \text{K}$, $10\,\text{K}$ will change the position of heat current maximums from $V_p = -40.3\ \ \text{V}$ and $V_p = 13.9\,\text{V}$ to $V_p = -13\,\text{V}$. Hence, one can modulate the piezo voltage V_p to control the magnitude of heat currents, and this system can realize the function of a heat valve. What is more important, it is also found that heat currents exhibit nonreciprocal heat transfer from Figs. 3(a) and 3(b), which means that this system can also be implemented as a thermal diode. The rectification factor can characterize the performance of the nonreciprocal heat

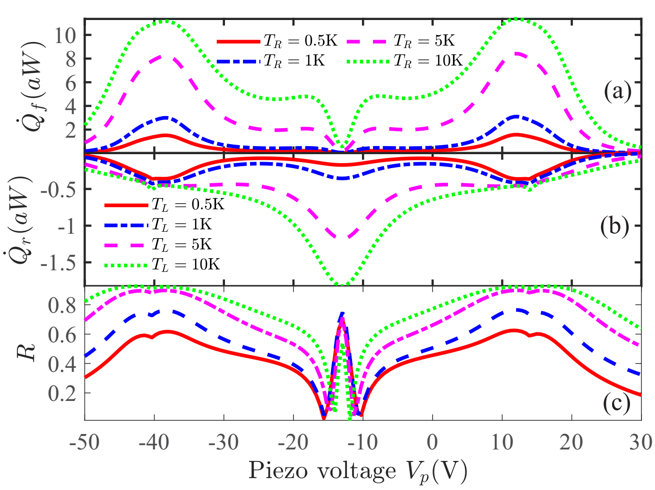

FIG. 3. The forward (a), reverse (b) heat currents, and rectification coefficient (c) versus the applied piezo voltage. The related parameters: dissipation rates $\gamma_L/2\pi = 3\,\text{MHz}$, $\gamma_R = \gamma_L$, and temperatures $T_{L/R} = 0.1\,\text{K}$ for the forward and reverse transfer, respectively, and other parameters are the same as in Fig. 2.

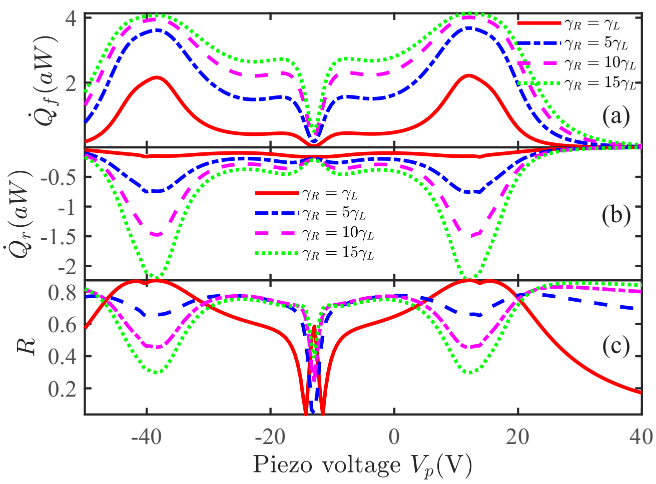

FIG. 4. The forward (a), reverse (b) heat currents, and rectification coefficient (c) versus the applied voltage for different system-reservoir couplings. System parameters: dissipation rates $\gamma_L/2\pi = 1\,\text{MHz}$; In forward process, temperatures take $T_L = 0.1\,\text{K}$, $T_R = 3\ \ \text{K}$; In reverse process $T_L = 0.1\ \ \text{K}$, $T_R = 3\,\text{K}$, and other parameters are the same as in Fig. 2.

transport rectification factor. The rectification factor versus voltage V_p is shown in Fig. 3(c), and nearly perfect rectification can be approximately obtained at $V_p \approx -40.3\ \ \text{V}$ and $V_p \approx 13.9\,\text{V}$ at large temperature difference. However, at the two points $V_p \approx -14\ \text{V}, -11\ \text{V}$, the rectification effects approach zero. This can be understood as follows. Note that $\gamma_R = \gamma_L$ isn't enough to mean the symmetric system-reservoir coupling because of the potential different transition channels and operators as shown in Eq. (A1). In this sense, one can roughly understand the asymmetry of atomic interaction and the asymmetry system-reservoir couplings could offset, which leads to the reciprocal heat transfer at the two particular points. A subtle analysis is given in Appendix C.

As mentioned previously, different system-reservoir couplings are an important factor in realizing a heat rectification effect [44,64]. Next, we will show whether the performance of the thermal diode can be boosted using the different system-reservoir coupling strengths in Fig. 4. It is found that the stronger asymmetric coupling strength can realize the larger heat transport. Moreover, the performance of heat diodes employing asymmetric and symmetric couplings can be complementary. In comparison of the equal system-reservoir coupling strength, for $\omega_R = \omega_L$ the rectification effects at $V_p = -40.3\,\text{V}$ and $V_p = 13.9\ \ \text{V}$ are weakened, which can also be attributed to the competition of the asymmetry of atomic interaction and the asymmetry of the system-reservoir couplings. The rectification at $V_p \approx -13\ \ \text{V}$ in Fig. 4 can also be understood similarly. In addition, the nearly stable rectification effect can be obtained at $V_p \in [-30, -15], [-10, 5], [20, 40]\ \ \text{V}$. To explain this result, we give the population number as a function of V_p as shown in Fig. 5. We find that in these ranges, populations ρ_{11}, ρ_{44} are dominantly for forward heat transfer, while ρ'_{11}, ρ'_{33} play the main role for reverse process. It means that the transition channel $|\epsilon_1\rangle \leftrightarrow |\epsilon_4\rangle$, $|\epsilon_2\rangle \leftrightarrow |\epsilon_1\rangle$ of forward transfer is different than reverse process $|\epsilon_1\rangle \leftrightarrow |\epsilon_3\rangle$, $|\epsilon_2\rangle \leftrightarrow |\epsilon_1\rangle$, and it

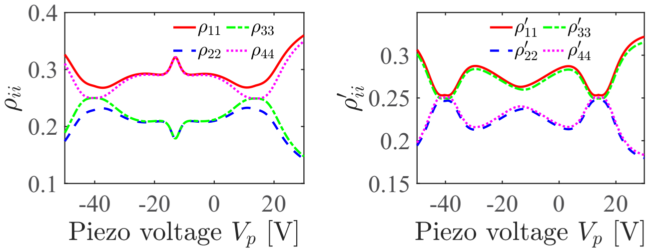

(a) (b)

FIG. 5. The forward (a) and reverse (b) populations as a function of the piezo voltage when considering the different coupling strengths of system reservoir. Parameters: dissipation rates $\gamma_L/2\pi = 1$ MHz, $\gamma_R = 5\gamma_L$; $T_L = 0.1$ K, $T_R = 5$ K for forward process; $T_R = 5$ K, $T_L = 0.1$ K for reverse process, and other parameters as shown in Fig. 2.

may enable directional heat flow. Besides, we also researched the temperature-modulated heat valve and diode with different voltages V_p. From Fig. 6, we find that there is no heat current when temperatures of two terminals are equal $T_R = T_L$, and the higher temperature bias is beneficial to heat rectification. The rectification effect's mechanism stems from the asymmetry of energy structure, as shown in Fig. 2. In summary, one can realize a well-performaning diode in a wide parameter range.

The occurrence of the rectification effect requires some asymmetry of the total system. No rectification effect exists when the total system, including heat reservoirs, is fully symmetric, i.e., the same asymmetry energy ε_μ, tunneling energy Δ_μ, and system-reservoir couplings for the current system. To explain the reason for the heat rectification effect shown in Fig. 6. The existence of different energy structures

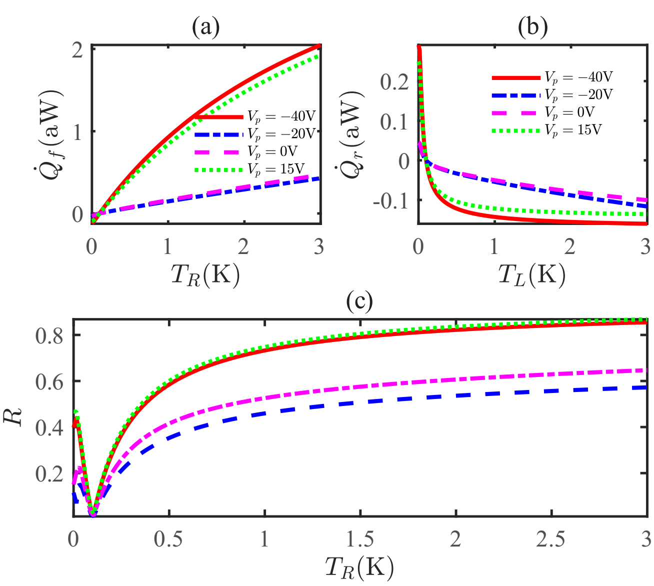

FIG. 6. The forward (a), reverse (b) heat currents, and rectification coefficient (c) versus the temperatures for different voltage V_p. System parameters: dissipation rates $\gamma_L/2\pi = 3$ MHz, $\gamma_R = \gamma_L$; In forward process, temperatures take $T_L = 0.1$ K; In reverse process $T_R = 0.1$ K, and other parameters are the same as in Fig. 2.

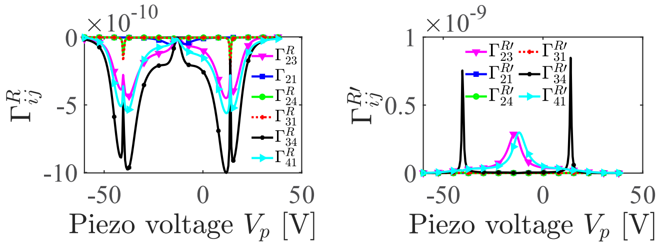

(a) (b)

FIG. 7. The transition rates for the forward (a) and reverse (b) versus the applied piezo voltage. Parameters: $\gamma_L/2\pi = 3$ MHz, $\gamma_R = \gamma_L$; $T_L = 0.1$ K, $T_R = 5$ K for forward process; $T_R = 5$ K, $T_L = 0.1$ K for reverse process, and other parameters as shown in Fig. 2.

of atoms induced by modulation of piezo voltage and different tunneling provides the asymmetry to realize nonreciprocal heat transport, as shown in Fig. 2(b). It involves the same six transition channels for each atom with independent reservoir $|\epsilon_2\rangle \leftrightarrow |\epsilon_3\rangle$, $|\epsilon_2\rangle \leftrightarrow |\epsilon_1\rangle$, $|\epsilon_2\rangle \leftrightarrow |\epsilon_4\rangle$, $|\epsilon_3\rangle \leftrightarrow |\epsilon_1\rangle$, $|\epsilon_3\rangle \leftrightarrow |\epsilon_4\rangle$, and $|\epsilon_4\rangle \leftrightarrow |\epsilon_1\rangle$, but the coefficient of transition rates are different [cf. Eq. (A1)]. Meanwhile, the two terminals have different temperatures, providing the various transition abilities of the same channel. For example, we take a transition channel $|\epsilon_1\rangle \leftrightarrow |\epsilon_4\rangle \leftrightarrow |\epsilon_3\rangle \leftrightarrow |\epsilon_2\rangle \leftrightarrow |\epsilon_1\rangle$. When we consider the forward transfer $T_L < T_R$, the higher temperature T_R can realize $|\epsilon_1\rangle \rightarrow |\epsilon_4\rangle \rightarrow |\epsilon_3\rangle \rightarrow |\epsilon_2\rangle$, however, when we invert the temperatures of the two terminals, the lower temperature T_R have insufficient ability to fulfill it. From this perspective, it is found that the reverse heat transport is a blockade. From Eq. (18), heat current is the sum of the product of transition rate and transition energy. To further understand the rectification effect, we plot the transition rates as a function of piezo voltage shown in Fig. 7. We are comparing Figs. 7(a) and 7(b); the transition rates with the same transition energy are different for forward and reverse transfer, which causes nonreciprocal heat transport. Here, we also consider it analytically and obtain a solution at low temperatures shown in Appendix A. Figure 8 exhibits approximate heat

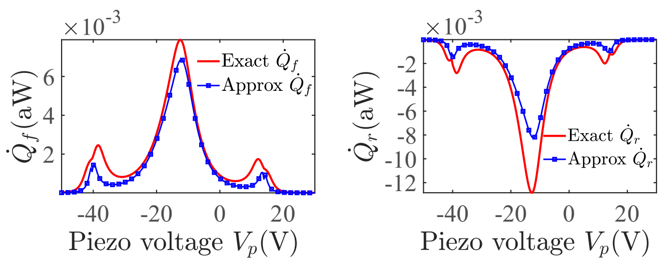

(a) (b)

FIG. 8. Heat currents as a function of piezo voltage V_p for forward (a) and reverse (b) heat transfer. The red solid line and blue squared line denote the exact [cf. Eq. (18)] and approximate heat currents [cf. Eq. (B5)], respectively. Here $\gamma_L/2\pi = 3$ MHz, $\gamma_R = \gamma_L$; temperatures take $T_L = 5$ mK, $T_R = 10$ mK for forward transfer, otherwise exchanging temperature of two terminals of the reservoir. Other parameters are the same as shown in Fig. 2.

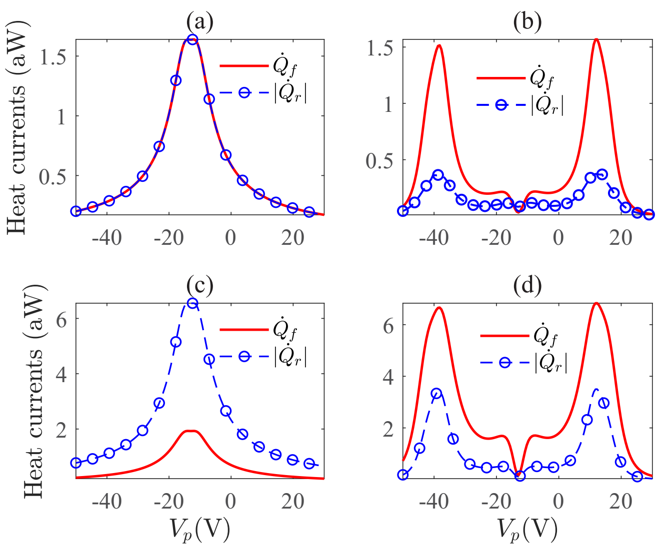

FIG. 9. The forward and reverse heat currents as a function of the applied piezo voltage V_p with four different cases considering asymmetry of total system including environment. (a) Full symmetry, $\Delta_L = \Delta_R$, $\gamma_R = \gamma_L$, and $\varepsilon_R = \varepsilon_L$; (b) Different energy structures ε_μ and Δ_μ, $\varepsilon_L = c_L V_p - 3.3$ [GHz], $\Delta_L = 7.5$ GHz; (c) Different system-reservoir coupling strength $\gamma_R = 10\gamma_L$; (d) Different energy structures ε_μ and Δ_μ and system-reservoir coupling strength γ_μ, $\varepsilon_L = c_L V_p - 3.3$ [GHz], $\Delta_L = 7.5$ GHz, and $\gamma_R = 10\gamma_L$. The other parameters: In the forward process $T_L = 0.1$ K, $T_R = 0.5$ K; In the reverse process $T_R = 0.1$ K, $T_L = 0.5$ K, $g = 850$ MHz, $\Delta_R = 1.3$ GHz, $\gamma_L/2\pi = 3$ MHz, $c_L = 5$ MHzV^{-1}, $c_R = 0.3$ GHzV^{-1}, and $\varepsilon_R(V_p) = c_R(V_p + 13[\mathrm{V}])$.

current [cf. Eq. (B5) for forward and reverse heat transfer in comparison to the exact case, cf. Eq. (18)]. Although the magnitude of the heat current is small, it provides an analytical form to understand the nonreciprocal heat transport. The approximate heat currents are valid in a wide region from this figure. A heat valve can realize this regardless of the forward and reverse transfer. One also finds that nonreciprocal heat transport can occur when we invert the temperatures of two terminals. From Eq. (B5), one can find that it provides the same result when exchanging the temperatures of two terminals.

Finally, we would like to consider the proposal's feasibility. The two coupling two-level system defects can be realized in the AlOx of Josephson junction tunnel barriers. Each atom can be coupled to a normal-metal resistor [44] or general noiseless resistor with a fluctuating voltage source [53,54] act as a thermal bath. The setup of tuning a two-level system by applied mechanical strain has been extensively discussed in Refs. [47,65]. The two-level system relaxation rates $\gamma_\mu/2\pi$ can be taken in the range 0.1–5 MHz [48]. In addition, heat current can be detected by employing the normal-metal-insulator-superconductor (NIS) thermometry techniques [38,66].

IV. CONCLUSION AND DISCUSSION

We have theoretically proposed a heat valve and diode via modulating the piezo voltage in a defect coupling atoms system. It is shown that a well-performing heat valve and diode can be realized at an extensive parameter range. We discuss the effect of piezo voltage, temperature, and system-reservoir coupling strength on the performance of heat devices and give a physical explanation for the phenomena. We hope this work can provide an efficient way to design and modulate quantum thermal rectification devices.

ACKNOWLEDGMENTS

This work was supported by the National Natural Science Foundation of China under Grants No.12175029, No. 12011530014, and No.11775040.

APPENDIX A: THE EIGENOPERATOR OF OPEN SYSTEM

In H_S representation, the jump operators S_μ of the system can be solved as

$$\begin{aligned}
S_{L1} &= \sin\theta_L \sin\left(\frac{\alpha+\beta}{2}\right)|\epsilon_3\rangle\langle\epsilon_2|,\\
S_{L2} &= -\cos\theta_L \sin\alpha|\epsilon_1\rangle\langle\epsilon_2|,\\
S_{L3} &= \sin\theta_L \cos\left(\frac{\alpha+\beta}{2}\right)|\epsilon_4\rangle\langle\epsilon_2|,\\
S_{L4} &= \sin\theta_L \cos\left(\frac{\alpha+\beta}{2}\right)|\epsilon_1\rangle\langle\epsilon_3|,\\
S_{L5} &= -\cos\theta_L \sin\beta|\epsilon_4\rangle\langle\epsilon_3|,\\
S_{L6} &= -\sin\theta_L \sin\left(\frac{\alpha+\beta}{2}\right)|\epsilon_1\rangle\langle\epsilon_4|,\\
S_{R1} &= \sin\theta_R \cos\left(\frac{\alpha-\beta}{2}\right)|\epsilon_3\rangle\langle\epsilon_2|,\\
S_{R2} &= -\cos\theta_R \sin\alpha|\epsilon_1\rangle\langle\epsilon_2|,\\
S_{R3} &= \sin\theta_R \sin\left(\frac{\alpha-\beta}{2}\right)|\epsilon_4\rangle\langle\epsilon_2|,\\
S_{R4} &= -\sin\theta_R \sin\left(\frac{\alpha-\beta}{2}\right)|\epsilon_1\rangle\langle\epsilon_3|,\\
S_{R5} &= \cos\theta_R \sin\beta|\epsilon_4\rangle\langle\epsilon_3|,\\
S_{R6} &= \sin\theta_R \cos\left(\frac{\alpha-\beta}{2}\right)|\epsilon_1\rangle\langle\epsilon_4|,\\
S_{L0} &= \cos\theta_L \cos\alpha(|\epsilon_3\rangle\langle\epsilon_3| - |\epsilon_2\rangle\langle\epsilon_2|)\\
&\quad + \cos\theta_L \cos\beta(|\epsilon_1\rangle\langle\epsilon_1| - |\epsilon_4\rangle\langle\epsilon_4|),\\
S_{R0} &= \cos\theta_R \cos\alpha(|\epsilon_3\rangle\langle\epsilon_3| - |\epsilon_2\rangle\langle\epsilon_2|)\\
&\quad + \cos\theta_R \cos\beta(|\epsilon_4\rangle\langle\epsilon_4| - |\epsilon_1\rangle\langle\epsilon_1|).
\end{aligned} \tag{A1}$$

The corresponding eigenfrequencies are $\omega_{\mu1} = \omega_{32} = \epsilon_2 - \epsilon_3$, $\omega_{\mu2} = \omega_{12} = \epsilon_2 - \epsilon_1$, $\omega_{\mu3} = \omega_{42} = \epsilon_2 - \epsilon_4$, $\omega_{\mu4} = \omega_{13} = \epsilon_3 - \epsilon_1$, $\omega_{\mu5} = \omega_{43} = \epsilon_3 - \epsilon_4$, and $\omega_{\mu6} = \omega_{14} = \epsilon_4 - \epsilon_1$. Here we tab the coefficient of $S_{\mu l}$ as $a_{\mu l}$, for example, $a_{L1} = \sin\theta_L \sin(\frac{\alpha+\beta}{2})$.

APPENDIX B: THE POPULATION, AND HEAT CURRENT FOR COUPLED SYSTEM

The density matrix for the composite system at steady state can be solved as

$$\begin{aligned}
\rho_{11} &= ((A_4+A_5+B_1)(A_3A_6+A_2(A_6+B_3))+(A_3A_4+A_2(A_4+B_1))B_5+A_1(A_5A_6+A_4(A_6+B_3+B_5)))/N,\\
\rho_{22} &= (A_5A_6B_2+(A_4B_2+B_1(B_2+B_4))(A_6+B_3+B_5)+A_4B_3B_6+B_1(B_3+B_5)B_6+A_5B_3(B_2+B_4+B_6))/N,\\
\rho_{33} &= (A_3A_6B_4+(A_2B_4+A_1(B_2+B_4))(A_6+B_3+B_5)+A_2B_5B_6+A_1(B_3+B_5)B_6+A_3B_5(B_2+B_4+B_6))/N,\\
\rho_{44} &= (A_2A_5B_4+A_1A_5(B_2+B_4)+(A_1+A_2)(A_4+A_5)B_6+A_2B_1B_6+A_3A_4(B_2+B_6)+A_3(A_5+B_1)(B_2+B_4+B_6))/N.
\end{aligned} \tag{B1}$$

Here N denotes the normalized coefficient, $A_i=\sum_\mu A_{\mu i}$, and $B_i=\sum_\mu B_{\mu i}$. To obtain an analytical expression, we consider low temperatures. It means $e^{-\frac{\omega}{T_L}}, e^{-\frac{\omega}{T_R}} \ll 1$ and the involved transition are $|\epsilon_2\rangle \leftrightarrow |\epsilon_3\rangle$, $|\epsilon_3\rangle \leftrightarrow |\epsilon_4\rangle$, and $|\epsilon_4\rangle \leftrightarrow |\epsilon_1\rangle$. For simplification, we take $\gamma=\gamma_L$ and $\kappa=\gamma_R$. Based on those conditions, one can simplify matrix M with normalized condition $\mathrm{Tr}(\rho)=1$ as

$$M_m=\begin{pmatrix} M_m^{11} & 0 & 0 & 2a_{L6}^2\gamma+2a_{R6}^2\kappa\\ 0 & -2a_{L1}^2\gamma-2a_{R1}^2\kappa & 2a_{L1}^2e^{\frac{-\omega_{32}}{T_L}}\gamma+2a_{R1}^2e^{\frac{-\omega_{32}}{T_R}}\kappa & 0\\ 2a_{R4}^2e^{\frac{-\omega_{13}}{T_R}}\kappa & 2a_{L1}^2\gamma+2a_{R1}^2\kappa & M_m^{33} & 2a_{L5}^2e^{\frac{-\omega_{43}}{T_L}}\gamma+2a_{R5}^2e^{\frac{-\omega_{43}}{T_R}}\kappa\\ 1 & 1 & 1 & 1 \end{pmatrix}, \tag{B2}$$

where $M_m^{11}=-2a_{R4}^2e^{\frac{-\omega_{13}}{T_R}}\kappa-2a_{R6}^2e^{-\frac{-\omega_{14}}{T_R}}\kappa$, and $M_m^{33}=-2a_{L5}^2\gamma-2a_{R5}^2\kappa-2a_{L1}^2e^{\frac{-\omega_{32}}{T_L}}\gamma-2a_{R1}^2e^{\frac{-\omega_{32}}{T_R}}\kappa$. The matrix determinant of M_m can be expressed as

$$\begin{aligned}
\mathrm{Det}(M_m) = 8e^{-\frac{(T_L+T_R)(\epsilon_2+\epsilon_3+\epsilon_4)}{T_LT_R}}\Big(&-\big(e^{\frac{\epsilon_2}{T_R}+\frac{\epsilon_3}{T_L}}\gamma a_{L1}^2+e^{\frac{\epsilon_2}{T_L}+\frac{\epsilon_3}{T_R}}\kappa a_{R1}^2\big)\big(\big(e^{\frac{\epsilon_3}{T_R}+\frac{\epsilon_4}{T_L}}\gamma a_{L5}^2+e^{\frac{\epsilon_3}{T_L}+\frac{\epsilon_4}{T_R}}\kappa a_{R5}^2\big)\big(e^{\frac{\epsilon_1}{T_L}+\frac{\epsilon_4}{T_R}}\gamma a_{L6}^2\\
&+\big(e^{\frac{\epsilon_1}{T_L}+\frac{\epsilon_4}{T_R}}\gamma a_{L6}^2+e^{\frac{\epsilon_1}{T_R}+\frac{\epsilon_4}{T_L}}\big(e^{\frac{\epsilon_1}{T_L}+\frac{\epsilon_4}{T_R}}\gamma a_{L6}^2+\big(e^{\frac{\epsilon_1}{T_L}+\frac{\epsilon_4}{T_R}}\gamma a_{L6}^2+e^{\frac{\epsilon_1}{T_R}+\frac{\epsilon_4}{T_L}}\kappa a_{\mathrm{R6}}^2\big)-e^{\frac{(T_L+T_R)\epsilon_3}{T_LT_R}}\big(\gamma a_{L1}^2+\kappa a_{R1}^2\big)\\
&\times\big(e^{\frac{\epsilon_4}{T_R}}\big(e^{\frac{\epsilon_1}{T_L}}+e^{\frac{\epsilon_4}{T_L}}\big)\gamma a_{L6}^2+e^{\frac{\epsilon_4}{T_L}}\big(e^{\frac{\epsilon_1}{T_R}}+e^{\frac{\epsilon_4}{T_R}}\big)\kappa a_{R6}^2\big)\big)-\big(\gamma a_{L1}^2+\kappa a_{R1}^2\big)\big(e^{\frac{(T_L+T_R)\epsilon_2}{T_LT_R}}\big(e^{\frac{\epsilon_3}{T_R}+\frac{\epsilon_4}{T_L}}\gamma a_{L5}^2+e^{\frac{\epsilon_3}{T_L}+\frac{\epsilon_4}{T_R}}\kappa a_{R5}^2\big)\\
&\times\big(e^{\frac{\epsilon_1}{T_L}+\frac{\epsilon_4}{T_R}}\gamma a_{L6}^2+e^{\frac{\epsilon_1}{T_R}+\frac{\epsilon_4}{T_L}}\kappa a_{\mathrm{R6}}^2\big)+e^{\frac{(T_L+T_R)\epsilon_3}{T_LT_R}}\big(e^{\frac{\epsilon_2}{T_R}+\frac{\epsilon_3}{T_L}}\gamma a_{L1}^2+e^{\frac{\epsilon_2}{T_L}}\big(e^{\frac{\epsilon_3}{T_R}}\kappa a_{R1}^2+e^{\frac{\epsilon_2}{T_R}}\big(\gamma a_{L5}^2+\kappa a_{R5}^2\big)\big)\big)\\
&\times\big(e^{\frac{\epsilon_4}{T_R}}\big(e^{\frac{\epsilon_1}{T_L}}+e^{\frac{\epsilon_4}{T_L}}\big)\gamma a_{L6}^2+e^{\frac{\epsilon_4}{T_L}}\big(e^{\frac{\epsilon_1}{T_R}}+e^{\frac{\epsilon_4}{T_R}})\kappa a_{R6}^2\big)\big)\Big).
\end{aligned} \tag{B3}$$

The corresponding steady state can be approximately solved as

$$\begin{aligned}
\rho_{11} &= -\frac{8\big(\gamma a_{L1}^2+\kappa a_{R1}^2\big)\big(\gamma a_{L5}^2+\kappa a_{R5}^2\big)\big(\gamma a_{L6}^2+\kappa a_{R6}^2\big)}{\mathrm{Det}(M_m)},\\
\rho_{22} &= -\frac{8e^{-\frac{(T_L+T_R)(\epsilon_2+\epsilon_3+\epsilon_4)}{T_LT_R}}\big(e^{\frac{\epsilon_2}{T_R}+\frac{\epsilon_3}{T_L}}\gamma a_{L1}^2+e^{\frac{\epsilon_2}{T_L}+\frac{\epsilon_3}{T_R}}\kappa a_{R1}^2\big)\big(e^{\frac{\epsilon_3}{T_R}+\frac{\epsilon_4}{T_L}}\gamma a_{L5}^2+e^{\frac{\epsilon_3}{T_L}+\frac{\epsilon_4}{T_R}}\kappa a_{R5}^2\big)\big(e^{\frac{\epsilon_1}{T_L}+\frac{\epsilon_4}{T_R}}\gamma a_{L6}^2+e^{\frac{\epsilon_1}{T_R}+\frac{\epsilon_4}{T_L}}\kappa a_{R6}^2\big)}{\mathrm{Det}(M_m)},\\
\rho_{33} &= -\frac{8e^{-\frac{(T_L+T_R)(\epsilon_3+\epsilon_4)}{T_LT_R}}\big(\gamma a_{L1}^2+\kappa a_{R1}^2\big)\big(e^{\frac{\epsilon_3}{T_R}+\frac{\epsilon_4}{T_L}}\gamma a_{L5}^2+e^{\frac{\epsilon_3}{T_L}+\frac{\epsilon_4}{T_R}}\kappa a_{R5}^2\big)\big(e^{\frac{\epsilon_1}{T_L}+\frac{\epsilon_4}{T_R}}\gamma a_{L6}^2+e^{\frac{\epsilon_1}{T_R}+\frac{\epsilon_4}{T_L}}\kappa a_{R6}^2\big)}{\mathrm{Det}(M_m)},\\
\rho_{44} &= -\frac{8e^{-\frac{(T_L+T_R)\epsilon_4}{T_LT_R}}\big(\gamma a_{L1}^2+\kappa a_{R1}^2\big)\big(\gamma a_{L5}^2+\kappa a_{R5}^2\big)\big(e^{\frac{\epsilon_1}{T_L}+\frac{\epsilon_4}{T_R}}\gamma a_{L6}^2+e^{\frac{\epsilon_1}{T_R}+\frac{\epsilon_4}{T_L}}\kappa a_{R6}^2\big)}{\mathrm{Det}(M_m)}.
\end{aligned} \tag{B4}$$

According to the definition of heat current Eq. (18) and the above equations, one can obtain an approximate expression as

$$\begin{aligned}
\dot{\mathcal{Q}}_R = 8\Big(&2e^{-\frac{(T_L+T_R)(\epsilon_2+\epsilon_3+\epsilon_4)}{T_LT_R}}\kappa a_{R1}^2\big(e^{\frac{\epsilon_2}{T_R}+\frac{\epsilon_3}{T_L}}\gamma a_{L1}^2+e^{\frac{\epsilon_2}{T_L}+\frac{\epsilon_3}{T_R}}\kappa a_{R1}^2\big)\big(e^{\frac{\epsilon_3}{T_R}+\frac{\epsilon_4}{T_L}}\gamma a_{L5}^2+e^{\frac{\epsilon_3}{T_L}+\frac{\epsilon_4}{T_R}}\kappa a_{R5}^2\big)\big(e^{\frac{\epsilon_1}{T_L}+\frac{\epsilon_4}{T_R}}\gamma a_{L6}^2\\
&+e^{\frac{\epsilon_1}{T_R}+\frac{\epsilon_4}{T_L}}\kappa a_{R6}^2\big)(\epsilon_2-\epsilon_3)+e^{-\frac{T_L\epsilon_2+(T_L+T_R)(\epsilon_3+\epsilon_4)}{T_LT_R}}\kappa\big(\gamma a_{L1}^2+\kappa a_{R1}^2\big)\big(e^{\frac{\epsilon_3}{T_R}+\frac{\epsilon_4}{T_L}}\gamma a_{L5}^2+e^{\frac{\epsilon_3}{T_L}+\frac{\epsilon_4}{T_R}}\kappa a_{R5}^2\big)\big(e^{\frac{\epsilon_1}{T_L}+\frac{\epsilon_4}{T_R}}\gamma a_{L6}^2\\
&+e^{\frac{\epsilon_1}{T_R}+\frac{\epsilon_4}{T_L}}\kappa a_{R6}^2\big)\big(e^{\frac{\epsilon_3}{T_R}}a_{R1}^2(-\epsilon_2+\epsilon_3\big)+e^{\frac{\epsilon_2}{T_R}}a_{R5}^2(\epsilon_3-\epsilon_4))+2e^{\frac{\epsilon_1-\epsilon_4}{T_R}}\kappa\big(\gamma a_{L1}^2+\kappa a_{R1}^2\big)\big(\gamma a_{L5}^2+\kappa a_{R5}^2\big)a_{R6}^2(\gamma a_{L6}^2\\
&+\kappa a_{R6}^2)(\epsilon_1-\epsilon_4)+2e^{-\frac{T_L\epsilon_3+(T_L+T_R)\epsilon_4}{T_LT_R}}\kappa\big(\gamma a_{L1}^2+\kappa a_{R1}^2\big)\big(\gamma a_{L5}^2+\kappa a_{R5}^2\big)\big(e^{\frac{\epsilon_1}{T_L}+\frac{\epsilon_4}{T_R}}\gamma a_{L6}^2+e^{\frac{\epsilon_1}{T_R}+\frac{\epsilon_4}{T_L}}\kappa a_{R6}^2\big)\\
&\times\big(-e^{\frac{\epsilon_3}{T_R}}a_{R6}^2(\epsilon_1-\epsilon_4\big)+e^{\frac{\epsilon_4}{T_R}}a_{R5}^2(-\epsilon_3+\epsilon_4)\big)\Big)/\mathrm{Det}(M_m).
\end{aligned} \tag{B5}$$

APPENDIX C: HEAT RECTIFICATION EFFECTS INDUCED BY THE ASYMMETRY OF TOTAL SYSTEM INCLUDING ENVIRONMENT

We will analyze four cases for different total system structures to understand the thermal rectification effect more intuitively. In general, the asymmetry of the total system includes the asymmetry of subsystems and the asymmetry of the system reservoir. As shown in Fig. 9, we have plotted heat currents versus the V_p with different asymmetry mechanisms. Compared to Fig. 9(a), all other figures can have heat rectification effects. From Figs. 9(b) and 9(d), we find that the different system energy structures in some ranges may lead to weak rectification, and different energy structures and system-reservoir coupling strength can produce competition in realizing heat rectification. Besides, one only considers the different system-reservoir coupling strengths shown in Fig. 9(c), the rectification can also be enhanced.

[1] J. P. Pekola and B. Karimi, Colloquium: Quantum heat transport in condensed matter systems, Rev. Mod. Phys. **93**, 041001 (2021).
[2] J.-Q. You and F. Nori, Atomic physics and quantum optics using superconducting circuits, Nature (London) **474**, 589 (2011).
[3] M. H. Devoret and R. J. Schoelkopf, Superconducting circuits for quantum information: An outlook, Science **339**, 1169 (2013).
[4] P.-M. Billangeon, J. S. Tsai, and Y. Nakamura, Circuit-QED-based scalable architectures for quantum information processing with superconducting qubits, Phys. Rev. B **91**, 094517 (2015).
[5] A. Gubaydullin, G. Thomas, D. S. Golubev, D. Lvov, J. T. Peltonen, and J. P. Pekola, Photonic heat transport in three terminal superconducting circuit, Nat. Commun. **13**, 1552 (2022).
[6] S. Vinjanampathy and J. Anders, Quantum thermodynamics, Contemp. Phys. **57**, 545 (2016).
[7] M. J. Martínez-Pérez, A. Fornieri, and F. Giazotto, Rectification of electronic heat current by a hybrid thermal diode, Nat. Nanotechnol. **10**, 303 (2015).
[8] N. Linden, S. Popescu, and P. Skrzypczyk, How small can thermal machines be? The smallest possible refrigerator, Phys. Rev. Lett. **105**, 130401 (2010).
[9] A. Levy and R. Kosloff, Quantum absorption refrigerator, Phys. Rev. Lett. **108**, 070604 (2012).
[10] C.-s. Yu and Q.-y. Zhu, Re-examining the self-contained quantum refrigerator in the strong-coupling regime, Phys. Rev. E **90**, 052142 (2014).
[11] J. B. Brask, G. Haack, N. Brunner, and M. Huber, Autonomous quantum thermal machine for generating steady-state entanglement, New J. Phys. **17**, 113029 (2015).
[12] P. P. Hofer, M. Perarnau-Llobet, J. B. Brask, R. Silva, M. Huber, and N. Brunner, Autonomous quantum refrigerator in a circuit QED architecture based on a Josephson junction, Phys. Rev. B **94**, 235420 (2016).
[13] F. Ivander, N. Anto-Sztrikacs, and D. Segal, Strong system-bath coupling effects in quantum absorption refrigerators, Phys. Rev. E **105**, 034112 (2022).
[14] D. Kolisnyk and G. Schaller, Performance boost of a collective qutrit refrigerator, Phys. Rev. Appl. **19**, 034023 (2023).
[15] L. Tesser, B. Bhandari, P. A. Erdman, E. Paladino, R. Fazio, and F. Taddei, Heat rectification through single and coupled quantum dots, New J. Phys. **24**, 035001 (2022).
[16] J. Ordonez-Miranda, Y. Ezzahri, and K. Joulain, Quantum thermal diode based on two interacting spinlike systems under different excitations, Phys. Rev. E **95**, 022128 (2017).
[17] T. Werlang, M. A. Marchiori, M. F. Cornelio, and D. Valente, Optimal rectification in the ultrastrong coupling regime, Phys. Rev. E **89**, 062109 (2014).
[18] G. T. Landi, E. Novais, M. J. de Oliveira, and D. Karevski, Flux rectification in the quantum XXZ chain, Phys. Rev. E **90**, 042142 (2014).
[19] V. Balachandran, G. Benenti, E. Pereira, G. Casati, and D. Poletti, Perfect diode in quantum spin chains, Phys. Rev. Lett. **120**, 200603 (2018).
[20] V. Balachandran, G. Benenti, E. Pereira, G. Casati, and D. Poletti, Heat current rectification in segmented XXZ chains, Phys. Rev. E **99**, 032136 (2019).
[21] K. Poulsen, A. C. Santos, L. B. Kristensen, and N. T. Zinner, Entanglement-enhanced quantum rectification, Phys. Rev. A **105**, 052605 (2022).
[22] T. Ruokola, T. Ojanen, and A.-P. Jauho, Thermal rectification in nonlinear quantum circuits, Phys. Rev. B **79**, 144306 (2009).
[23] M. Xu, J. T. Stockburger, and J. Ankerhold, Heat transport through a superconducting artificial atom, Phys. Rev. B **103**, 104304 (2021).
[24] A. A. Aligia, D. P. Daroca, L. Arrachea, and P. Roura-Bas, Heat current across a capacitively coupled double quantum dot, Phys. Rev. B **101**, 075417 (2020).
[25] C. Kargı, M. T. Naseem, T. Opatrný, O. E. Müstecaplıoğlu, and G. Kurizki, Quantum optical two-atom thermal diode, Phys. Rev. E **99**, 042121 (2019).
[26] Z.-X. Man and Y.-J. Xia, Smallest quantum thermal machine: The effect of strong coupling and distributed thermal tasks, Phys. Rev. E **96**, 012122 (2017).
[27] A. Iorio, E. Strambini, G. Haack, M. Campisi, and F. Giazotto, Photonic heat rectification in a system of coupled qubits, Phys. Rev. Appl. **15**, 054050 (2021).
[28] Y.-q. Liu, Y.-j. Yang, and C.-s. Yu, Quantum heat diode versus light emission in circuit quantum electrodynamical system, Phys. Rev. E **107**, 044121 (2023).
[29] K. Joulain, J. Drevillon, Y. Ezzahri, and J. Ordonez-Miranda, Quantum thermal transistor, Phys. Rev. Lett. **116**, 200601 (2016).
[30] B.-Q. Guo, T. Liu, and C.-S. Yu, Quantum thermal transistor based on qubit-qutrit coupling, Phys. Rev. E **98**, 022118 (2018).
[31] N. Gupt, S. Bhattacharyya, B. Das, S. Datta, V. Mukherjee, and A. Ghosh, Floquet quantum thermal transistor, Phys. Rev. E **106**, 024110 (2022).
[32] M. Majland, K. S. Christensen, and N. T. Zinner, Quantum thermal transistor in superconducting circuits, Phys. Rev. B **101**, 184510 (2020).

[33] B.-Q. Guo, T. Liu, and C.-S. Yu, Multifunctional quantum thermal device utilizing three qubits, Phys. Rev. E **99**, 032112 (2019).

[34] J. Lu, R. Wang, J. Ren, M. Kulkarni, and J.-H. Jiang, Quantum-dot circuit-QED thermoelectric diodes and transistors, Phys. Rev. B **99**, 035129 (2019).

[35] C. Wang, X.-M. Chen, K.-W. Sun, and J. Ren, Heat amplification and negative differential thermal conductance in a strongly coupled nonequilibrium spin-boson system, Phys. Rev. A **97**, 052112 (2018).

[36] P. P. Hofer, J. B. Brask, M. Perarnau-Llobet, and N. Brunner, Quantum thermal machine as a thermometer, Phys. Rev. Lett. **119**, 090603 (2017).

[37] R. T. Wijesekara, S. D. Gunapala, and M. Premaratne, Towards quantum thermal multi-transistor systems: Energy divider formalism, Phys. Rev. B **105**, 235412 (2022).

[38] A. Ronzani, B. Karimi, J. Senior, Y.-C. Chang, J. T. Peltonen, C. Chen, and J. P. Pekola, Tunable photonic heat transport in a quantum heat valve, Nat. Phys. **14**, 991 (2018).

[39] Y.-q. Liu, Y.-j. Yang, T.-t. Ma, and C.-s. Yu, Quantum heat valve and entanglement in superconducting LC resonators, Appl. Phys. Lett. **123**, 144002 (2023).

[40] Y.-Q. Liu, D.-H. Yu, and C.-S. Yu, Common environmental effects on quantum thermal transistor, Entropy **24**, 32 (2021).

[41] Y.-j. Yang, Y.-q. Liu, and C.-s. Yu, Quantum thermal diode dominated by pure classical correlation via three triangular-coupled qubits, Phys. Rev. E **107**, 064125 (2023).

[42] P. Portugal, C. Flindt, and N. Lo Gullo, Heat transport in a two-level system driven by a time-dependent temperature, Phys. Rev. B **104**, 205420 (2021).

[43] B. Karimi, J. Pekola, M. Campisi, and R. Fazio, Coupled qubits as a quantum heat switch, Quantum Sci. Technol. **2**, 044007 (2017).

[44] J. Senior, A. Gubaydullin, B. Karimi, J. T. Peltonen, J. Ankerhold, and J. P. Pekola, Heat rectification via a superconducting artificial atom, Commun. Phys. **3**, 40 (2020).

[45] J. Lisenfeld, G. J. Grabovskij, C. Müller, J. H. Cole, G. Weiss, and A. V. Ustinov, Observation of directly interacting coherent two-level systems in an amorphous material, Nat. Commun. **6**, 6182 (2015).

[46] C. Müller, J. H. Cole, and J. Lisenfeld, Towards understanding two-level-systems in amorphous solids: Insights from quantum circuits, Rep. Prog. Phys. **82**, 124501 (2019).

[47] G. J. Grabovskij, T. Peichl, J. Lisenfeld, G. Weiss, and A. V. Ustinov, Strain tuning of individual atomic tunneling systems detected by a superconducting qubit, Science **338**, 232 (2012).

[48] T. Ramos, V. Sudhir, K. Stannigel, P. Zoller, and T. J. Kippenberg, Nonlinear quantum optomechanics via individual intrinsic two-level defects, Phys. Rev. Lett. **110**, 193602 (2013).

[49] S. M. Meißner, A. Seiler, J. Lisenfeld, A. V. Ustinov, and G. Weiss, Probing individual tunneling fluctuators with coherently controlled tunneling systems, Phys. Rev. B **97**, 180505(R) (2018).

[50] O. de los Santos-Sánchez and R. Román-Ancheyta, Strain-spectroscopy of strongly interacting defects in superconducting qubits, Supercond. Sci. Technol. **35**, 035005 (2022).

[51] J. Lisenfeld, A. Bilmes, S. Matityahu, S. Zanker, M. Marthaler, M. Schechter, G. Schön, A. Shnirman, G. Weiss, and A. V. Ustinov, Decoherence spectroscopy with individual two-level tunneling defects, Sci. Rep. **6**, 23786 (2016).

[52] A. J. Leggett, S. Chakravarty, A. T. Dorsey, M. P. A. Fisher, A. Garg, and W. Zwerger, Dynamics of the dissipative two-state system, Rev. Mod. Phys. **59**, 1 (1987).

[53] A. A. Clerk, M. H. Devoret, S. M. Girvin, F. Marquardt, and R. J. Schoelkopf, Introduction to quantum noise, measurement, and amplification, Rev. Mod. Phys. **82**, 1155 (2010).

[54] M. Cattaneo and G. S. Paraoanu, Engineering dissipation with resistive elements in circuit quantum electrodynamics, Adv. Quantum Technol. **4**, 2100054 (2021).

[55] A. J. Leggett, Quantum tunneling in the presence of an arbitrary linear dissipation mechanism, Phys. Rev. B **30**, 1208 (1984).

[56] E. Paladino, M. Sassetti, G. Falci, and U. Weiss, Characterization of coherent impurity effects in solid-state qubits, Phys. Rev. B **77**, 041303(R) (2008).

[57] G. M. Reuther, D. Zueco, F. Deppe, E. Hoffmann, E. P. Menzel, T. Weißl, M. Mariantoni, S. Kohler, A. Marx, E. Solano, R. Gross, and P. Hänggi, Two-resonator circuit quantum electrodynamics: Dissipative theory, Phys. Rev. B **81**, 144510 (2010).

[58] L. G. Remus, M. P. Blencowe, and Y. Tanaka, Damping and decoherence of a nanomechanical resonator due to a few two-level systems, Phys. Rev. B **80**, 174103 (2009).

[59] I. de Vega and D. Alonso, Dynamics of non-Markovian open quantum systems, Rev. Mod. Phys. **89**, 015001 (2017).

[60] H.-P. Breuer and F. Petruccione, *The Theory of Open Quantum Systems* (Oxford University Press, Oxford, 2002).

[61] A. Levy, R. Alicki, and R. Kosloff, Quantum refrigerators and the third law of thermodynamics, Phys. Rev. E **85**, 061126 (2012).

[62] G. Schaller, *Open Quantum Systems Far from Equilibrium*, Vol. 881 (Springer, 2014).

[63] S. Matityahu, J. Lisenfeld, A. Bilmes, A. Shnirman, G. Weiss, A. V. Ustinov, and M. Schechter, Rabi noise spectroscopy of individual two-level tunneling defects, Phys. Rev. B **95**, 241409(R) (2017).

[64] D. Segal and A. Nitzan, Spin-boson thermal rectifier, Phys. Rev. Lett. **94**, 034301 (2005).

[65] A. Bilmes, S. Volosheniuk, J. D. Brehm, A. V. Ustinov, and J. Lisenfeld, Quantum sensors for microscopic tunneling systems, npj Quantum Inf. **7**, 27 (2021).

[66] F. Giazotto, T. T. Heikkilä, A. Luukanen, A. M. Savin, and J. P. Pekola, Opportunities for mesoscopics in thermometry and refrigeration: Physics and applications, Rev. Mod. Phys. **78**, 217 (2006).